Renewable Energy 145 (2020) 2192–2200

Contents lists available at ScienceDirect

Renewable Energy

journal homepage: www.elsevier.com/locate/renene

Improving performance and stability in quantum dot-sensitized solar cell through single layer graphene/Cu_2S nanocomposite counter electrode

Erdi Akman [a, b], Yemliha Altintas [c], Mahir Gulen [d], Mucahit Yilmaz [e], Evren Mutlugun [f, g], Savas Sonmezoglu [a, h, *]

[a] Nanotechnology R&D Laboratory, Karamanoglu Mehmetbey University, Karaman, Turkey
[b] Department of Mechanical Engineering, Konya Technical University, Konya, Turkey
[c] Department of Materials Science and Nanotechnology Engineering, Abdullah Gul University, Kayseri, Turkey
[d] Department of Mechanical Engineering, Bartin University, Bartin, Turkey
[e] Department of Physics, Necmettin Erbakan University, Konya, Turkey
[f] Department of Electrical & Electronics Engineering, Abdullah Gul University, Kayseri, Turkey
[g] UNAM, Institute of Materials Science and Nanotechnology, Bilkent University, Ankara, Turkey
[h] Department of Metallurgical and Materials Engineering, Karamanoglu Mehmetbey University, Karaman, Turkey

ARTICLE INFO

Article history:
Received 1 December 2018
Received in revised form
1 June 2019
Accepted 29 July 2019
Available online 30 July 2019

Keywords:
Quantum-dot sensitized solar cell (QDSSC)
Single layer graphene and Cu_2S film
Counter electrode
Electrodeposition method
Chemical vapor deposition

ABSTRACT

In this work, we presented an effective nanocomposite to modify the Cu_2S film by employing single layer graphene (SLG) frameworks via chemical vapor deposition, and utilized this nanocomposite as counter electrode (CE) with CdSe/ZnS core/shell quantum dots for highly stable and efficient quantum dot-sensitized solar cell (QDSSC). Furthermore, Cu_2S film is directly synthesized on SLG framework by electrodeposition method. Using this nanocomposite as CE, we have achieved the high efficiency as high as 3.93% with fill factor of 0.63, which is higher than those with bare Cu_2S CE (3.40% and 0.57). This remarkable performance is attributed to the surface area enhancement by creating nanoflower-shape, the reduction of charge transfer resistance, improvement of catalytic stability, and the surface smoothness as well as good adhesion. More importantly, no visible color change and detachment from surface for the Cu_2S@SLG nanocomposite was observed, demonstrating that the SLG framework is critical role in shielding the Cu_2S structure from sulphur ions into electrolyte, and increasing the adhesion of the Cu_2S structure on surface, thus preventing its degradation. Consequently, the Cu_2S@SLG nanocomposite can be utilized as an effective agent to boost up the performance of QDSSCs.

1. Introduction

Quantum dot-sensitized solar cells (QDSSCs) have attracted considerable attention in recent years, owing to their tunable band gap, low-cost, easy-fabrication procedure and high theoretically reported power conversion efficiency (PCE) up to 44% [1]. The photoelectrochemical mechanism of QDSSCs exhibits similar behavior to dye-sensitized solar cells (DSSCs), in which the QDs is used instead of the dye molecules as a light absorber layer in QDSSCs [2]. Typically, QDSSC is assembled by a quantum dots-sensitized photoanode film, an electrolyte with the inclusion of a redox couple (i.e. S^{2-}/S_x^{2-}) and a counter electrode (CE) (i.e. Pt, and Cu_2S) [1–3]. Despite these advantages, however, the photovoltaic performance of most QDSSCs is still much lower than those obtained from DSSCs. In order to improve the cell performance, till date many research work has focused on optimizing all the components in QDSSCs. Since one of the main reasons for low efficiency is the loss at electrolyte–counter electrode interfaces, particularly the research efforts have concentrated on the development of compatible CEs for achieving simultaneous high efficiency and stable cells.

Therefore, CEs are amongst the most critical components of the DSSCs since they are utilized to collect charge carriers from the external circuits and provide the reduction of redox electrolyte.

* Corresponding author. Nanotechnology R&D Laboratory, Karamanoglu Mehmetbey University, Karaman, Turkey.
E-mail address: svssonmezoglu@gmail.com (S. Sonmezoglu).

https://doi.org/10.1016/j.renene.2019.07.150
0960-1481/

Although platinum (Pt) has a considerably high electrocatalytic activity for iodide/triiodide redox couple in DSSCs [4–9], the utilization of this material in QDSSCs was not successful, as the adsorption of the sulfur on their surface leads to an increment of overpotential, the inefficient interface catalytic activity and low conductivity [10,11]. These factors result in lower current density and fill factor for the QDSSCs [12]. It is therefore necessary to search for alternative Pt-free materials compatible with polysulfide electrolyte as new CEs to further enhance the performance of QDSSCs. Till date, researchers have paid great effort in seeking alternative CE materials compatible with polysulfide electrolytes, such as Cu_xS [13,14], Cu_2S [15,16], CoS [17], PbS [18], Bi_2S_3 [19] and Cu_2ZnSnS_4 [20]. Among these materials, Cu_2S CEs on brass foil exhibit the highest electrocatalytic activity for reduction of polysulfide species in QDSSCs [1]. Although it appears to be the most effective material in QDSSCs, their charge carrier mobility and stability were not satisfactory, which is mainly due to the fact that the continual corrosion caused by the reaction with sulfide/polysulfide electrolyte over a long time period [21–24].

To avoid the aforementioned problems, the use of fluorine-doped tin oxide (FTO) conducting substrates has started instead of copper brass substrate to produce Cu_2S film. However, these substrates suffer from low electrical conductivity since Cu_2S has a poor conductivity. Therefore, it is of critical importance to attain high catalytic activity and conductivity by modified Cu_2S with conductive agents [25]. Recently, there has been a prominent trend of preparing composite CEs composed of graphene and Cu_2S to enhance the catalytic activity, efficiency and stability of QDSSCs. In 2011, such composite CE based on reduced graphene oxide (reduced-GO)-Cu_2S was reported by Kamat and co-workers, the corresponding properties were investigated [23]. In 2014, CEs composed of Cu_2S microspheres wrapped in reduced-GO nanosheets were introduced using solvothermal process [1] In 2016, Hessein's group reported hybrid Cu_xS/reduced-GO CEs using the one-pot hydrothermal method [22]. Recently, reduced-GO/Cu_2S composites have been presented to enhance the CE quality of the QDSSCs [25]. Although it is quite obvious that the composite CE possess remarkable electrocatalytic activity and stability, but the efficiency and the fill factor of these CEs still need to improve. In addition, from the industrial point of view, reduced-GO-based CEs require complex manufacturing routes; therefore they are not wisely attractive for mass production. Moreover, there are no reports yet focused on single layer graphene (SLG) grown by chemical vapor deposition (CVD) and Cu_2S composite material and their integration into CEs in QDSSCs. Comparing with other graphene-based materials, particularly, the multidirectional structure of CVD-grown SLG lead to many perfect performances, such as a large theoretical specific surface area, high-mechanical and thermal properties, corrosion resistance, a huge intrinsic electron mobility and excellent optical transmittance [26,27]. Therefore, we attempted to employ the CVD-grown as interlayer at Cu_2S/FTO interface due to the high surface area of the SLG, and thereby preventing Cu_2S detachment from substrates and passivating sulfur atoms. We speculate that this event has contributed performance and stability of QDSSCs.

In this work, for the first time, we have developed a one-step, highly stable, and electrocatalytically active Cu_2S@SLG nanocomposite CE on FTO substrate by a facile and scalable electrochemical method for CdSe/ZnS core/shell quantum dots based solar cells. Conductive SLG sheets act as a matrix to support Cu_2S nanoparticles, preventing their self-aggregation, which provides an increment of surface area with more active polysulfide reduction sites. Outstanding photovoltaic performance, a remarkably high PCE of 3.93% and FF of 0.63 was recorded in the case of using Cu_2S@SLG CE with excellent photostability under continuous operation. This significant photostability was ascribed to the comprehensive coverage of the Cu_2S nanoparticles with the SLG sheets, which is critical in protecting them from the polysulfide electrolyte corrosion.

2. Experimental methods

2.1. Synthesis of CdSe/ZnS core/shell quantum dots

Red-emitting CdSe/ZnS core/shell QDs are synthesized by modifying previously reported synthesis recipe [28–30]. Oleic acid (5 mL), Zn-acetate dihydrate (1.68 mmol) and CdO (1 mmol) chemicals are introduced 4-necked flask with a magnetic stirrer. Three times consecutive degassing with Ar-gas is successively applied to the reaction flask to remove impurities. The reaction vessel is heated to 140 °C and kept for 45 min at this temperature. Then, the flask is cooled to 50–60 °C and octadecene (25 mL) is injected into the solution under gas flow. After injection, the temperature of the solution is increased to 90 °C under vacuum, and then heated to 300 °C under Ar-gas atmosphere. 1M TOP-Se precursor (0.2 mL), which is prepared in glovebox, is swiftly injected into the flask under strong stirring and kept at this temperature for 80 s. After addition of 1-dodecanethiol (300 μL) in the solution, the system was kept for 20 min at 300 °C. At the end, 2 M TOP-S (1 mL) is injected slowly into the system and kept for 10 min. The solution is quickly cooled down using water bath. Hexane (5 mL) is added at 50 °C into the flask and the solution is centrifuged at 5000 rpm. Precipitate is discarded and ethanol added supernatant is precipitated with 5000 rpm for 10 min. Finally, the precipitate is dispersed in hexane.

2.2. Ligand exchange procedure from organic to water phase

Phase transfer from organic phase to water phase has been carried out by using ligand-exchange protocol which is a modified recipe from the literature [31] by using 3-mercaptopropionic acid (3-MPA) as follows:

As synthesized CdSe/ZnS QDs sample was cleaned two times with the mixture of acetone and methanol. Cleaned QDs were dispersed in 10 mL of fresh hexane and concentration of the sample was adjusted to 30 mg/mL, 40 mL of DI water and 15 mL of NH_4OH solution were added on CdSe/ZnS QDs and stirred at room temperature for 3 h. Following, 540 μL of 3-MPA was added on the mixture and kept overnight to realize ligand-exchange procedure efficiently with 3-MPA on the surface of the NCs. Then, the mixture was precipitated and cleaned with ethanol with the volume ratio as 4:1 (ethanol: mixture). The precipitate was dissolved in DI-water and used for device fabrication.

2.3. Synthesis of single layer graphene by chemical vapour deposition (CVD) and Cu_2S by electrochemical deposition technique

In briefly, SLG structures were deposited on polished Cu foils ($1.5 \times 1.5\ cm^2$ area and 25 μm thickness) by MTI OTF-1200 CVD system at 1000 °C, with gas mixture of CH_4 and H_2 (1:2 ratio) for 5 min. After that, SLG films on Cu foils were transferred on the F:SnO_2-coated (FTO) glass substrate(Asahi Glass, sheet resistance: 15 sq^{-1}). Prior to transfer, the FTO substrates were rinsed in an ultrasonic bath for 15 min with pure water, ethanol, acetone and again with pure water, respectively, and then dried by nitrogen flow. The transfer process was carried out by standard poly(methyl methacrylate) (PMMA) process. PMMA film was spin-coated on the SLG/copper foil, and the copper foil was removed by a $FeCl_3$ etchant. After that, the stack of SLG on PMMA was repeatedly washed by transferring to DI water. Washed FTO substrate was then placed on

top of the stack, lifted from the DI water on a piece of paper, and dried with nitrogen gas flow. Finally, the PMMA was etched by gentle soaking in acetone for 60 min and rinsed with isopropyl alcohol (IPA), and the resultant SLG/FTO sample dried at 60 °C in vacuum furnace for 30 min.

We utilized and modified the electrochemical deposition growth recipe reported by Xu et al. for Cu_2S CE on SLG framework [32]. In a standard synthesis, 3 mmol of $Cu(NO_3)_2$ and 3 mmol of $NaNO_3$ were mixed in 60 mL of DMSO. Later, 1.8 mmol of powder sulfur was slowly introduced into the solution. The sulfur was dissolved at 80 °C temperature and was kept at this level during the deposition process. The electrodeposition process was carried out with a potantiostat at −1.05 V under continuous stirring by using three electrode setup which includes Pt stick as CE, Ag/AgCl as reference electrode and SLG/FTO as working electrodes, respectively. After the deposition, prepared films were washed with once hot (at 50 °C) dimethyl sulfoxide (DMSO) and later with ethanol several times. As the last stage, prepared films were dried in vacuum furnace at 80 °C for 1 h.

2.4. Fabrication of CdSe/ZnS QDs sensitized solar cells

Mesoporous TiO_2 film was fabricated according to the previous report [33]. TiO_2 films were prepared using doctor-blading the TiO_2 paste on pre-cleaned FTO-glass. The film was then sintered at 500 °C for an hour for both the removal of the impurities and improving the crystallinity of the film. Then, synthesized CdSe/ZnS QDs were coated to the mesoporous TiO_2 films via drop wise by keeping 18 h under dark conditions. The polysulfide electrolyte was prepared by dissolving sulfur (1M) and sodium sulfide (1M) in DI water:methanol (v:v of 1:3 ratio) before each test. Cu_2S and Cu_2S@SLG CEs based solar cells were assembled using photoanodes, CEs and electrolyte as our previous report [33]. The electrolyte was synthesized freshly for each measurement.

2.5. Characterization

Photoluminescence (PL), absorption, structural and Fourier Transformation Infrared (FTIR) properties of CdSe/ZnS core/shell QDs were characterized by Agilent-Cary Eclipse fluorescence spectrophotometer, UV–Vis spectrometer (Thermo Genesys 10S), transmission electron microscope (TEM) (FEI Tecnai G2 F30) and Thermo Scientific Nicolet-6700 spectrometer, respectively. Structural properties of SLG films on FTO, Cu_2S and Cu_2S@SLG films were investigated by Renishaw-INVIA Reflex confocal Raman microscopy. TEM image and selected area X-ray diffraction (XRD-SAED) pattern of SLG were obtained by transferring SLG film on Ted pella 300 mesh copper grid. XRD patterns of Cu_2S CE were obtained using Bruker D8 advance with DAVINCI. Morphological properties of CEs were investigated using Tescan MAIA3 XMU model scanning electron microscope (SEM). Furthermore, elemental composition of Cu_2S film investigated by means of electron dispersive X-ray (EDX) spectroscopy, by using an attachment of SEM instrument. The electrochemical impedance spectroscopy (EIS) and cyclic voltammetry (CV) studies of CEs were conducted with potentiostat/galvanostat system (Ivium–compact Stat). The (J-V) curves of QDSSCs were measured with sourcemeter (Keithley 4200) under a standard solar irradiation of 300 W m^{-2} (Xe lamp with AM 1.5 filter). The wavelength-dependent incident photon to charge carrier efficiency (IPCE) was recorded by Enlitech QE-R equipped with a 75 W xenon arc lamp source. We further monitored the on-off plots of QDSSCs in chronoamperometry mode by alternately irradiating at 30 mW cm^{-2} and darkening the device for 180 s.

3. Results and discussions

Water-soluble CdSe/ZnS QDs were obtained by ligand-exchange procedure as described in Synthesis part. Average size of the QDs is about 6.2 nm which is calculated from TEM image as shown in Fig. 1A. Absorbance and (PL) spectra of the sample were given in Fig. 1B. Peak emission wavelength and FWMH of the synthesized water-soluble QDs are 613 nm and 31 nm, respectively. Quantum yield of the water-soluble CdSe/ZnS QDs were measured as 21% by relative QY measurement technique with Rh-6G.

Fig. 1C shows FTIR spectra of the 3-MPA-capped CdSe/ZnS core/shell QDs. The strongest band of absorption in the FTIR spectra was located at 3222 cm^{-1} and this band indicates the presence of -OH vibrations in 3-MPA. FTIR spectra of the pure 3-MPA has S-H absorption band at around 2568 cm^{-1}, which totally disappeared in 3-MPA-capped CdSe/ZnS QDs due to the bonding and coordinating of thiol group (-SH) on the QD surface [34,35]. Absorption peak at 1566 indicates C=O vibration. IR absorption bands of carboxyl group C-H vibrations observed at 2922-2851-1377and 1404 cm^{-1} [34–36]. All these IR absorption bands of 3-MPA-capped CdSe/ZnS core/shell QDs confirm that ligand exchange procedure successfully carried out by using 3-MPA.

To ascertain the overall quality of the SLG present on the FTO substrate, Raman maps were achieved from a (45×30 μm^2) of the graphene surface. The scaled Raman maps of D, G, 2D bands and I_{2D}/I_G ratio are exhibited in Fig. 2(A-D), respectively and corresponding to marked spots (circle, square and hexagonal), the characteristic graphene Raman spectra with D (~1340), G (~1580 cm^{-1}) and 2D (~2675 cm^{-1}) bands were demonstrated in Fig. 2E. The Raman spectra from all spots (Fig. 2E) shows characteristic features of SLG: (i) a ~2.5 intensity ratio of 2D–to–G (ii) a symmetric 2D band centered at ~2675 cm^{-1} with a full width half maximum (FWHM) of ~35 cm^{-1} [37,38]. Furthermore, as shown in Fig.2D, 2D–to–G ratio, which is above 2.5 over the whole surface, indicating the excellent quality and homogeneity of SLG film grown by CVD method on Cu foil and transferred to FTO substrate [39,40]. On the other hand, the Raman map of D band, which gives an idea about the defect levels in graphene, is uniform and close to the background signal, demonstrating that graphene films with larger domains possess a lower density of defects stem from nucleation centers or interdomains [41]. Moreover, as shown in Fig. 2E, the intensity of the D band is very low (for circle and square spots is absent) relative to intensity of 2D and G bands for all marked spots, showing that SLG structures have low defects and high quality in whole film.

The SEM image of SLG on FTO substrate is given in Fig. 2F. This figure clearly shows the boundary of the SLG. The higher-resolution SEM image shows the presence of SLG in Fig. 2F inset. The Fig. 2(G and H) show TEM image and SAED patterns of SLG film transferred to carbon-coated copper grids (Ted Pella), respectively. The TEM measurement shows that the as-obtained graphene sheets have a relatively smooth and planar structure (Fig. 2G), similar to that obtained by micromechanical cleavage and consist of up to a very large part SLG. Furthermore, one can see from the Fig. 2G there is no contrast difference in whole TEM image, confirming that the graphene formed as a single layer [42] The bottom right reveals its SAED pattern (Fig. 2H), showing a characteristic split dot set from a SLG sheet. In addition, multiple hexagonal diffraction patterns appear to indicate a wide range of dimensions of the parts forming the SLG film. The direct TEM imaging is fairly consistent with Raman results.

To investigate structural properties of Cu_2S and Cu_2S@SLG CEs, XRD and Raman measurements have been carried out. In Fig. 3A, the good match of the diffraction peaks of Cu_2S and the standard (JCPDS 26-1116) is presented. XRD pattern does not possess any

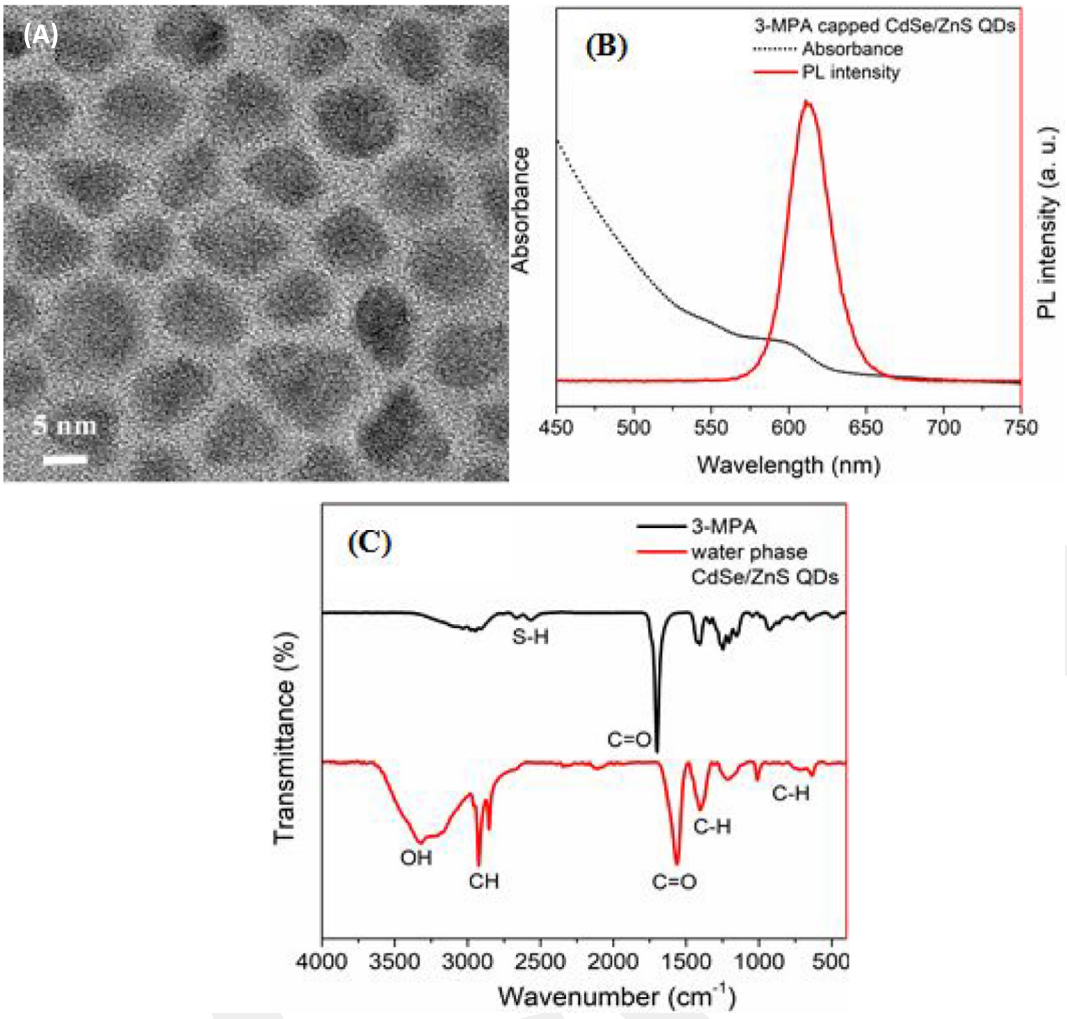

Fig. 1. (A) TEM images of the QDs **(B)** PL and Abs spectra of the water-soluble CdSe/ZnS core/shell QDs **(C)** FT-IR spectra of the pure 3-MPA and water phase 3-MPA-capped CdSe/ZnS QDs.

peaks from the bulk sulfur, which represents the formation of pure nanoparticles of chalcocite Cu_2S [43]. Furthermore, the crystallite size of the Cu_2S is calculated by determining the FWHM of main diffraction peak with Debye–Scherrer equation as ~14 nm. Fig. 3B shows the Raman spectra of the typical Cu_2S and Cu_2S@SLG films. This study revealed the Raman peaks of Cu_2S and Cu_2S@SLGare strong and sharp band at ~469.3and 471.5 cm^{-1}, which are in accordance with the results reported for Cu_2S [44,45]. As exhibited in Fig. 3B, by Cu_2S particles growing uniformly on the surface of SLG, Raman peak centered at 469.3 cm^{-1} shift to 471.5 cm^{-1} (up-shift), confirming that the interaction between Cu_2S crystal nucleus and carbon-oxygen groups of SLG structures [46,47]. This interaction proves that adhesiveness and electrical properties of Cu_2S film will improve.

To understand the effects of SLG on morphological properties and growth mechanism of the Cu_2S into composite matrix, SEM analyses were carried out. As demonstrated in Fig. 3C, while Cu_2S CE exhibits nanoparticles morphology, after incorporation of SLG into nanocomposite system the morphology changed to nano-flowers with the diameter of 0.5–0.7 μm. In the nanocomposite structure, copper and sulphur ions may accelerate immediately due to the excellent conductivity of SLG layer, resulting in fast and multiple nucleation of Cu_2S at the initial stage of the crystal growth [48,49]. Furthermore, every nucleus can grow up vertically along its orientation and consequently many of the growth orientations may have shaped flower-like 3-dimensional (3D) Cu_2S nano-architectures [50,51]. This change in morphology brings many advantages for Cu_2S@SLG nanocomposite film in CE applications. First, flower-like nanoarchitecture can provide larger surface area compare with particulate, leading to a larger interface contacting with the liquid electrolyte [52]. Second, flower-like nano-architecture can be expected as an effective charge transfer network facilitating the accumulation of the charge carriers from the external circuit and transfer of the charge carriers to liquid electrolyte, resulting in higher current density. Third, nanoflower-like CE with especially large surface area can decrease the charge transfer resistances and accelerate the diffusion of the liquid electrolyte, which are the responsible factors for the QDSSC performance [53]. Therefore, the CEs are expected to make an effective contribution to the performance of the QDSSCs. Furthermore, the composition of the electrodeposited Cu_2S nanostructure was investigated with EDX analysis. As shown in the Fig. 3E, the atomic ratio of Cu element is approximately being twice (~1.9) higher than that of S element, indicating that Cu_2S structure successfully synthesized by electrodeposition method.

The J–V characteristics of QDSSCs are shown in Fig. 4A and photovoltaic performance of QDSSCs were outlined in Table 1. As presented in Table 1, the open-circuit voltage (V_{oc}) values of the

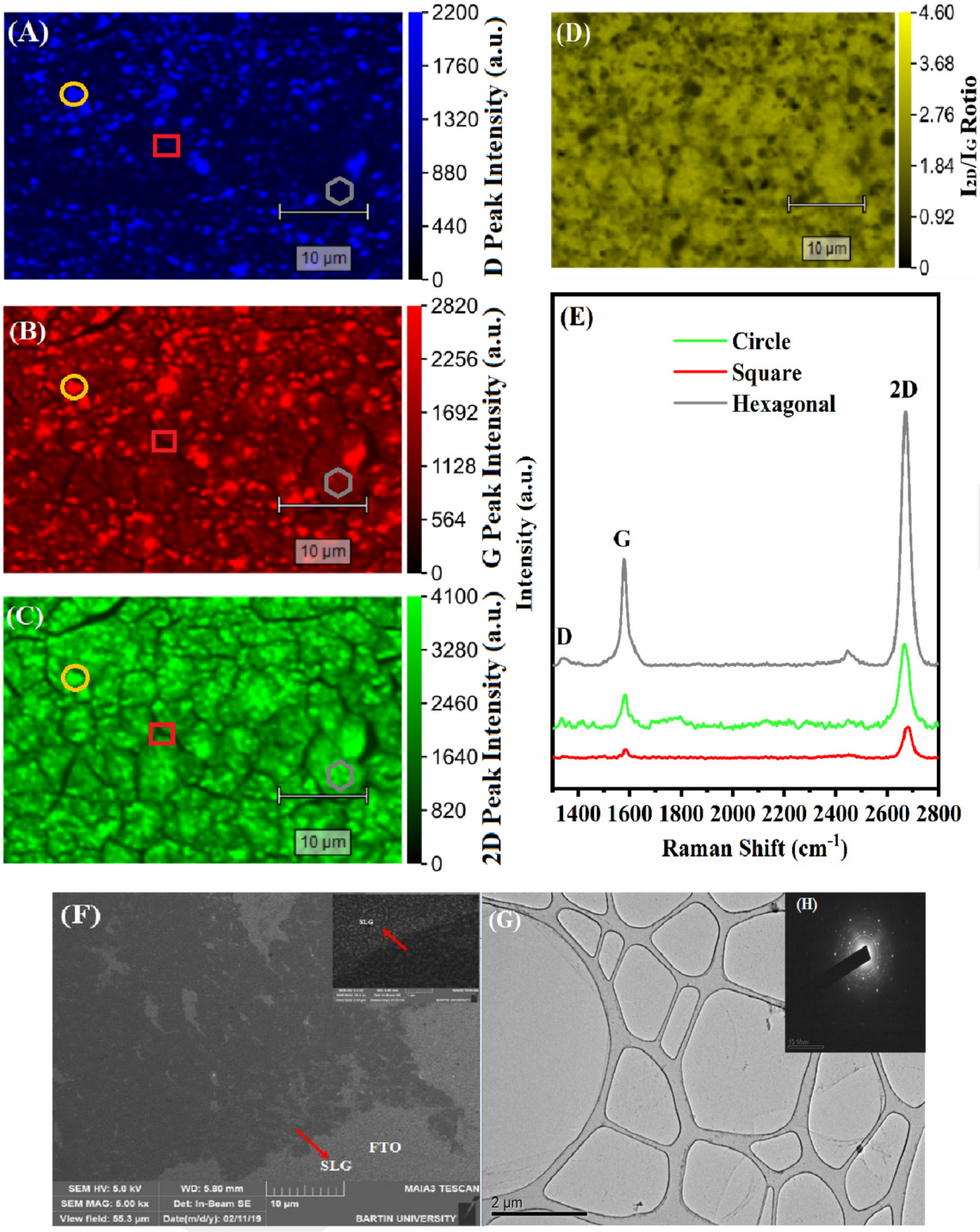

Fig. 2. **(A–D)** Raman maps of the D, G, 2D bands and I_{2D}/I_G ratio, respectively. **(E)** Raman spectra from the marked spots with corresponding colored geometrical shapes. **(F)** SEM image and **(G)** TEM images **(H)** SAED patterns of SLG structure.

resultant cells are nearly same with QDSSCs. Generally, V_{oc} is limited by the quasi-Fermi level of quantum dots sensitized TiO_2 and redox potential of electrolyte. In accordance, the QDSSC fabricated with Cu_2S@SLG CE possesses an overall efficiency (η) of 3.93%, which was much higher than that of Cu_2S CE, 3.40%. The increased PCE is primarily derived from the improvement of fill factor (FF) values combine with SLG material. This is attributed to the increment of charge transfer with conductively for Cu_2S@SLG CEs [54]. The obtained from the J–V curves, the short-circuit current density (J_{SC}) of 3.74 mA/cm^2 was obtained with Cu_2S@SLG CE in the QDSSCs. This value was slightly greater than this obtained Cu_2S CE (J_{SC} = 3.58 mA/cm^2).

As shown in Fig. 4B, the incident photon-to-current efficiency (IPCE) spectra were measured different photovoltaic performance of these two CEs between 350 and 700 nm wavelength regions. The IPCE value of Cu_2S@SLG based QDSSC at the wavelength region of 350–700 nm was about 45%, which was higher than Cu_2S QDSSC. This result agrees with the current density values of QDSSCs

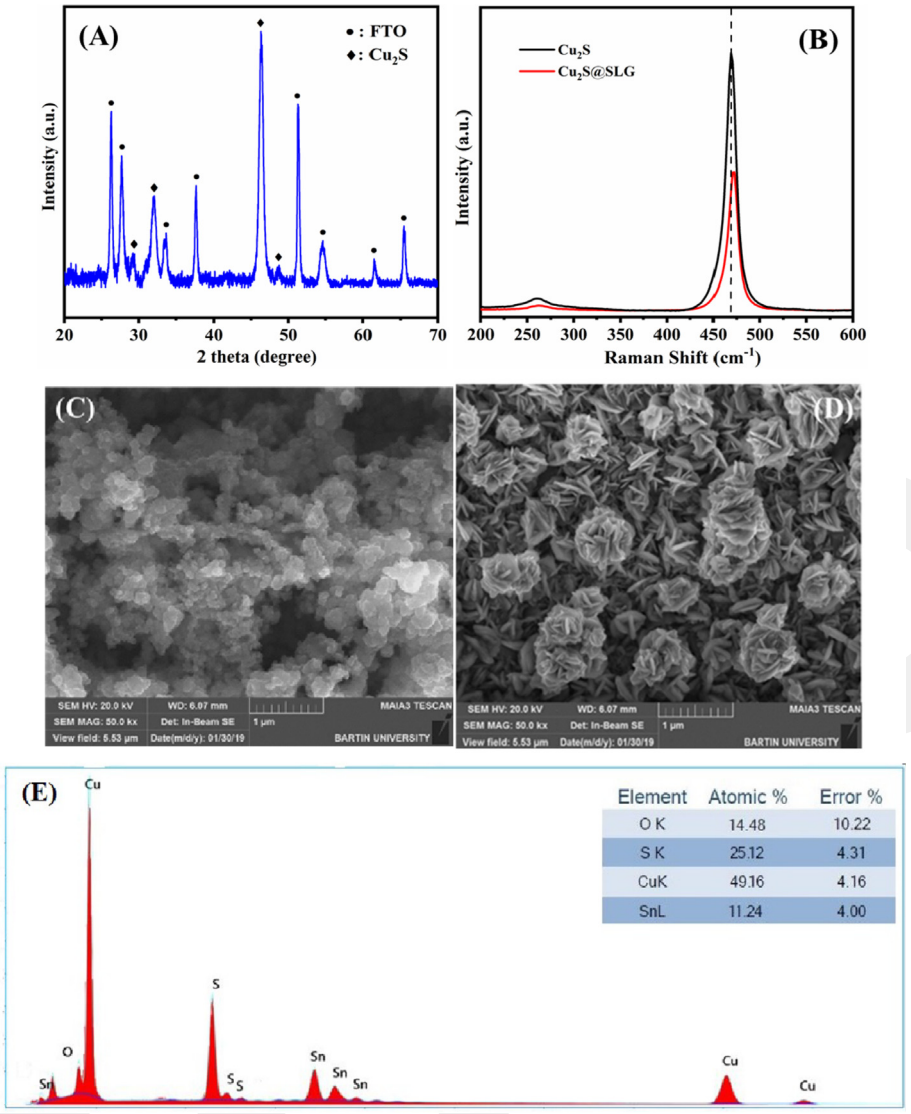

Fig. 3. **(A)** XRD pattern of Cu_2S on FTO substrate, **(B)** Raman spectra of Cu_2S on FTO substrate, **(C)** SEM images of Cu_2S film, **(D)** SEM images of Cu_2S@SLG nanocomposite films and (E) EDX of Cu_2S film.

presented (see Table 1). We can also infer from here that the Cu_2S@SLG layer and the FTO substrate have a better contact at their surface.

We have further conducted EIS measurements to monitor the catalytic activity of the CE, with a symmetrical cell constructed with two CEs (Cu_2S and Cu_2S@SLG). The equivalent circuit, including the series resistance (Rs), charge transfer resistance (R_{CT}) and interfacial capacitance (C), and resultant EIS plots of these different CEs are shown in Fig. 4C. The EIS parameters are outlined in Table 1. At the low-frequency, the charge transfer resistance (R_{CT2}), estimated by measuring the radius of second semicircle, give us information about CE/electrolyte interface. The R_{CT2} values of the Cu_2S and Cu_2S@SLG electrodes were 57.9 and 42.5 Ω, respectively. It clearly indicates that the Cu_2S@SLG CE has lower value of charge transfer resistance than Cu_2S CE. The fact that lower value of charge transfer resistance reflects the superior charge transfer and electrocatalytic ability at the CE/electrolyte interface [54]. The meaning difference is largely because the existence of SLG in Cu_2S@SLG composite can serve as an structure to firmly hold the Cu_2S nanostructure which also act as an efficient channel to transport charges which provided the improvement of electrocatalytic activity of Cu_2S@SLG electrode [1,23]. To examine the electrochemical catalytic activity of Cu_2S and Cu_2S@SLG CEs in polysulfide electrolyte, CV was performed, as shown in Fig. 4D. The relative catalytic activity of the obtained CEs can also be understood from the CV curve, by focusing on current density peak value. The negative current is attributed to the reduction reaction of Sn^{2-} to S^{2-}, and the positive current is attributed to the oxidation of S^{2-} in electrolyte [55,56]. The value of reduction peak current density (J_{red}) of Cu_2S@SLG CE is slightly higher than that of Cu_2S CE. As compared to the conventional Cu_2S CE the proposed Cu_2S@SLG CE structure has provide highly superior electrochemical stability and enhanced corrosion resistance [1,57]. Besides, one can see from Fig. 4D, Cu_2S@SLG CE possesses a lower peak-to-peak potential (E_{pp}) value than that of Cu_2S CE, exhibiting superior electrocatalytic activity of Cu_2S@SLG CE compare to Cu_2S [58].

The fast start-up and multiple start/stop cycling of QDSSCs are important to understand their photostability. In order to examine the repeatability of the device, photo-response study has been analyzed by chronoamperometry technique under light

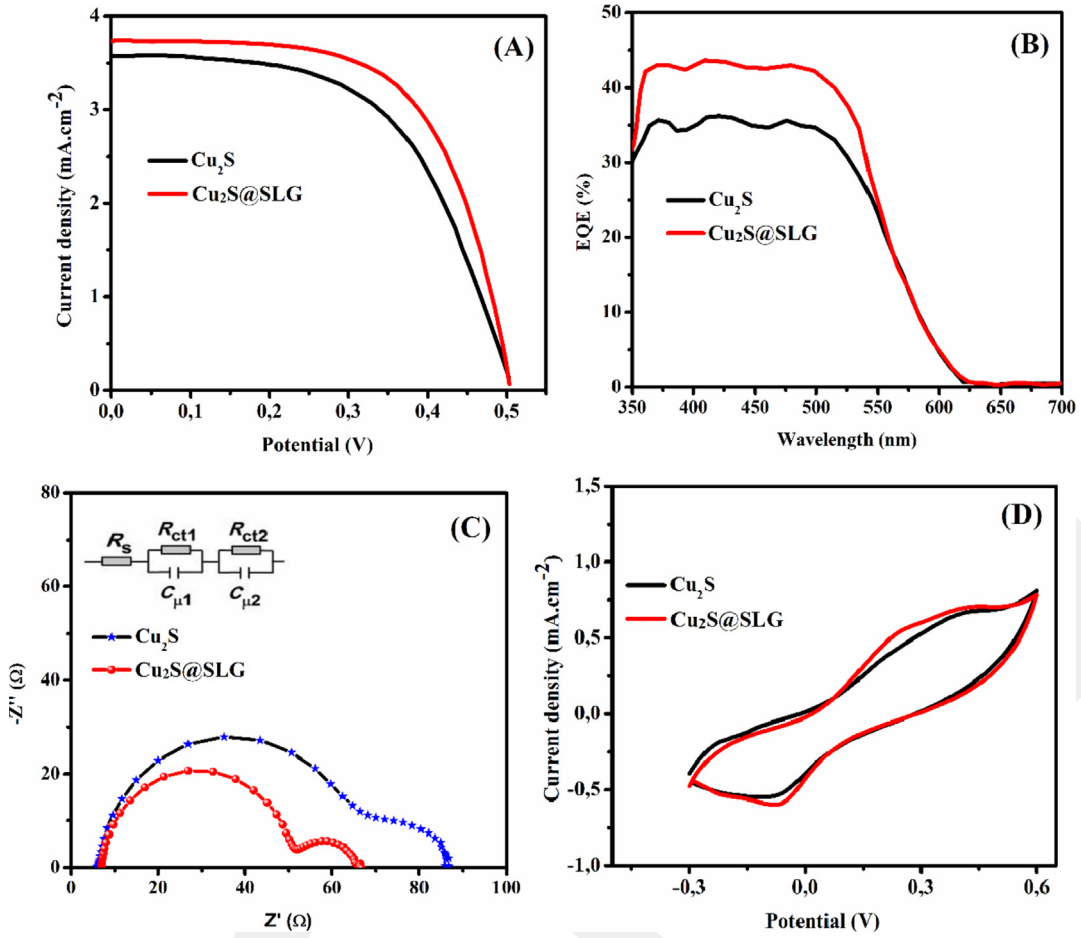

Fig. 4. **(A)** J–V characteristics, **(B)** IPCE spectra, **(C)** EIS measurements of QDSSCs, (**D**) CV of Cu_2S and Cu_2S@SLG CEs.

Table 1
EIS and photovoltaic performance of QDSSCs.

Samples	R_s (Ω)	R_{ct1} (Ω)	R_{ct2} (Ω)	C_1 (mF)	C_2 (mF)	J_{sc}(mA/cm^2)	V_{oc} (mV)	FF	η (%)
Cu_2S	7.17	57.90	20.00	130.0	10.70	3.58	0.50	0.57	3.40
Graphene/Cu_2S	7.65	43.50	13.30	517.0	7.42	3.74	0.50	0.63	3.93

illumination on/off for a total time of 180s when the polysulfide electrolyte is present and shown in Fig. 5A. When the light is turned on photocurrents are reached to 3.58 mA/cm^2 and 3.74 mA/cm^2 for Cu_2S CE and Cu_2S@SLG CE, respectively. The photocurrent-time curve observed for the QDSSCs are well agreement with its corresponding photocurrent-voltage character. Under illumination with light, a prompt and stable photocurrent density was observed in Cu_2S@SLG CE, implying that the collecting electron in Cu_2S@SLG can be rapidly transferred from CE to polysulfide electrolyte, which effectively prevents the recombination of electron-hole pairs. The QDSSC assembled with the Cu_2S CE suffered from instability as can be seen from the rapid drop in J_{SC} that reached about 85% after 180s light soaking. This drop was mainly due to the degradation and poisoning of the Cu_2S surface by sulfur ions. To examine the repeatability of the Cu_2S and Cu_2S@SLG CEs under certain irradiation, the J_{SC} of the assembled QDSSCs was also collected under irradiation around 180s. In Fig. 5B, the QDSSC with the Cu_2S@SLG as the CE exhibited no apparent change in J_{SC}, remaining ~98% of the initial value, during 180s, which shows its remarkable photostability. The achieved photostability of the QDSSC device was attributed to the high chemical durability of the Cu_2S@SLG CE which is due to the Cu_2S nanocrystals embedded within the SLG framework. On the other hand, the QDSSC based on the Cu_2S CE was not able to complete 180s photostability test. The J_{SC} was observed to be greatly suppressed. In comparison with the conventional Cu_2S CE, the results presented offers relatively better repeatability of the QDSSCs with a Cu_2S@SLG CE. Fig. 5C and D presents the color alteration of cells before/after exposing the polysulfide electrolyte. As presented in Fig. 5C and D, we have shown that the control devices degrade significantly within few hours, while the Cu_2S@SLG nanocomposite shows no discernible color change and detachment from surface, indicating that the SLG framework is critically important to protect the Cu_2S structure from sulphur ions penetrating into electrolyte, and to increase the adhesion of the Cu_2S structure on surface, thus preventing its degradation.

4. Conclusions

In this study, relatively highly electrocatalytic, repeatable and

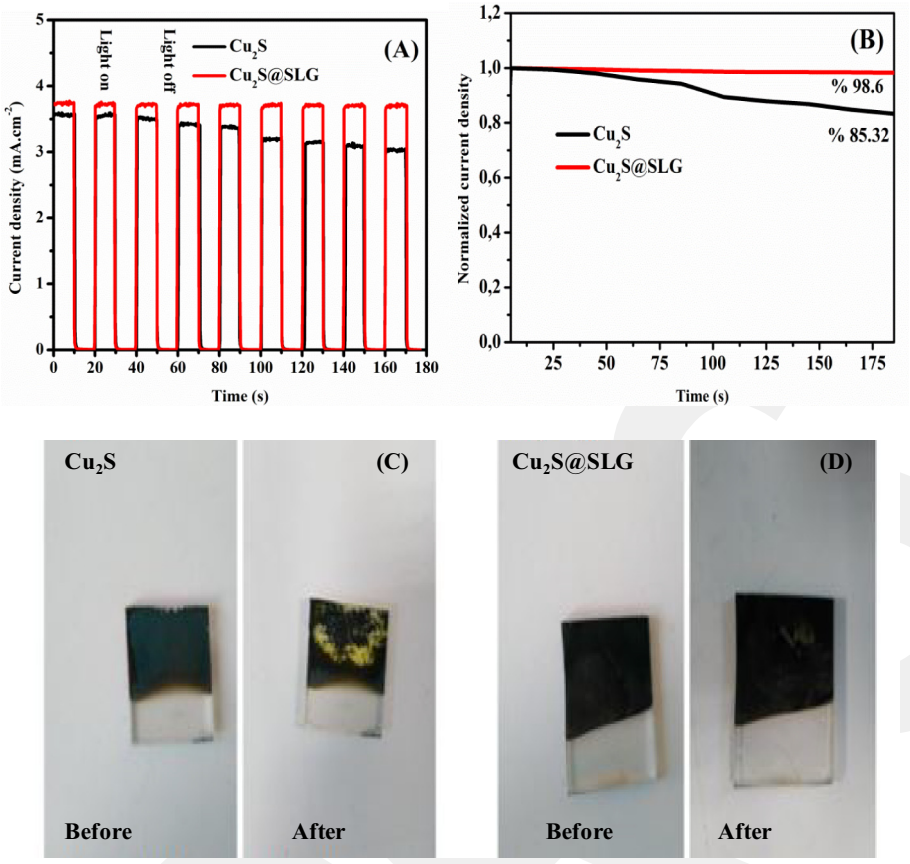

Fig. 5. **(A)** On-off test and **(B)** Time dependent stability of QDSSCs, and Digital pictures of **(C)** Cu_2S and **(D)** Cu_2S@SLG CEs before/after cell fabrication.

stable Cu_2S@SLG composite CE has been developed. The results indicated that with replacement of CE from Cu_2S to Cu_2S@SLG, J_{SC}, FF and η values shift from 3.58 mA/cm^2 to 3.74 mA/cm^2, 0.57 to 0.63 and 3.40%–3.93%, respectively. The development reasons of these photovoltaic parameters have been explained by EIS analysis, CV studies and the on-off test characterizations. The electrochemical measurements showed that the Cu_2S@SLG CE had superior electrocatalytic activity for polysulfide reduction to the Cu_2S CE. This is attributed to the large number of Cu_2S active sites and the rapid electron transport through the conductive SLG framework in the Cu_2S@SLG nanocomposite. Moreover, the repeatability measurement of the Cu_2S and Cu_2S@SLG CEs was examined for certain time. The obtained result indicates relatively more repeatability and stable of the solar cell with a Cu_2S@SLG CE in comparison to Cu_2S CE. All of the results have displayed a promising of Cu_2S@SLG composite employed as the CEs in QDSSCs.

Acknowledgement

The authors would like to thank Hanife Arslan and Bahri Eren Uzuner for they assistance during the experimental studies. EM acknowledges Turkish Academy of Sciences Distinguished Young Scientist Award (TUBA-GEBIP).

References

[1] M. Ye, C. Chen, N. Zhang, X. Wen, W. Guo, C. Lin, Quantum-dot sensitized solar cells employing hierarchical Cu_2S microspheres wrapped by reduced graphene oxide nanosheets as effective counter electrodes, Adv. Energy Mater. 4 (2014) 1301564–1301572.
[2] A. Hagfeldt, G. Boschloo, L.C. Sun, L. Kloo, H. Pettersson, Dye-sensitized solar cells, Chem. Rev. 110 (2010) 6595–6663.
[3] I. Hod, A. Zaban, Materials and interfaces in quantum dot sensitized solar cells: challenges, advances and prospects, Langmuir 25 (2014) 7264–7273.
[4] S. Akin, S. Sonmezoglu, Metal oxide nanoparticles as electron transport layer for highly efficient dye-sensitized solar cells, in: K.Y. Cheong, G. Impellizzeri, M.A. Fraga (Eds.), Emerging Materials for Energy Conversion and Storage, vol. 1, Elsevier, 2018, pp. 39–79.
[5] R. Tas, M. Can, S. Sonmezoglu, Exploring on photovoltaic performance of dye-sensitized solar cells using polyaniline as a counter electrode: role of aluminum-solvent interactions, IEEE J. Photovolt. 7 (2017) 792–801.
[6] R. Tas, M. Gulen, M. Can, S. Sonmezoglu, Effects of solvent and copper-doping on polyaniline conducting polymer and its application as a counter electrode for efficient and cost-effective dye-sensitized solar cells, Synth. Met. 212 (2016) 75–83.
[7] F. Ozel, A. Sarilmaz, B. Istanbullu, A. Aljabour, M. Kus, S. Sonmezoglu, Pentenary chalcogenides nanocrystals as catalytic materials for efficient counter electrodes in dye-synthesized solar cells, Sci. Rep. 6 (2016) 29207–29216.
[8] B. Bezgin Carbas, M. Gulen, M. Celik Tolu, S. Sonmezoglu, Hydrogen sulphate-based ionic liquid-assisted electro-polymerization of PEDOT catalyst material for high-efficiency photoelectrochemical solar cells, Sci. Rep. 7 (2017) 1–15.
[9] M. Gulen, A. Sarilmaz, I. Hatay Patir, F. Özel, S. Sonmezoglu, Ternary copper-tungsten-disulfide nanocube inks as catalyst for highly efficient dye-sensitized solar cells, Electrochim. Acta 269 (2018) 119–127.
[10] H. Chen, L. Zhu, H. Liu, W. Li, Efficient iron sulfide counter electrode for quantum dots-sensitized solar cells, J. Power Sources 245 (2014) 406–410.
[11] H.K. Jun, M.A. Careem, A.K. Arof, Quantum dot-sensitized solar cells-perspective and recent developments: a review of Cd chalcogenide quantum dots as sensitizers, Renew. Sustain. Energy Rev. 22 (2013) 148–167.
[12] V. Chakrapani, D. Baker, P.V. Kamat, Understanding the role of the sulfide redox couple (S^{2-}/Sn^{2-}) in quantum dot-sensitized solar cells, J. Am. Chem. Soc. 133 (2011) 9607–9615.
[13] D. Ghosh, G. Halder, A. Sahasrabudhe, S. Bhattacharyya, A microwave synthesized Cu_xS and graphene oxide nanoribbon composite as a highly efficient counter electrode for quantum dot sensitized solar cells, Nanoscale 8 (2016) 10632–10641.
[14] W. Chen, M. Wang, T. Qian, H. Cao, S. Huang, Q. He, N. Liang, C. Wang, J. Zai, Rational design and fabrication of skeletal Cu_7S_4 nanocages for efficient counter electrode in quantum dot-sensitized solar cells, Nano Energy 12 (2015) 186–196.
[15] M. Deng, S. Huang, Q. Zhang, D. Li, Y. Luo, Q. Shen, T. Toyoda, Q. Meng, Screen-printed Cu_2S-based counter electrode for quantum-dot-sensitized solar cell,

Chem. Lett. 39 (2010) 1168–1178.
[16] J.G.S. Selopal, I. Concina, R. Milan, M.M. Natile, G. Sberveglieri, A. Vomiero, Hierarchical self-assembled Cu_2S nanostructures: fast and reproducible spray deposition of effective counter electrodes for high efficiency quantum dot solar cells, Nano Energy 6 (2014) 200–210.
[17] M.L. Que, W.X. Guo, X.J. Zhang, X.Y. Li, Q.L. Hua, L. Dong, C.F. Pan, Flexible quantum dot-sensitized solar cells employing CoS nanorod arrays/graphite paper as effective counter electrodes, J. Mater. Chem. A 2 (2014) 13661–13666.
[18] C.Y. Lin, C.Y. Teng, T.L. Li, Y.L. Lee, H.S. Teng, Photoactive p-type PbS as a counter electrode for quantum dot-sensitized solar cells, J. Mater. Chem. A 1 (2013) 1155–1162.
[19] H.J. Yu, H.L. Bao, K. Zhao, Z.L. Du, H. Zhang, X.H. Zhong, Topotactically grown bismuth sulfide network film on substrate as low-cost counter electrodes for quantum dot-sensitized solar cells, J. Phys. Chem. C 118 (2014) 16602–16610.
[20] X. Zeng, W. Zhang, Y. Xie, D. Xiong, W. Chen, X. Xu, M. Wang, Y.-B. Cheng, Low-cost porous $Cu_2ZnSnSe_4$ film remarkably superior to noble Pt as counter electrode in quantum dot-sensitized solar cell system, J. Power Sources 226 (2013) 359–362.
[21] I. Hwang, K. Yong, Counter electrodes for quantum-dot-sensitized solar cells, ChemElectroChem. 2 (2015) 634–653.
[22] A. Hessein, F. Wang, H. Masai, K. Matsuda, A.A. El-Moneim, One-step fabrication of copper sulfide nanoparticles decorated on graphene sheets as highly stable and efficient counter electrode for CdS-sensitized solar cells, Jpn. App. Phys. 55 (2016) 112301–112309.
[23] J.G. Radich, R. Dwyer, P.V. Kamat, Cu_2S reduced graphene oxide composite for high-efficiency quantum dot solar cells: overcoming the redox limitations of S^{2-}/Sn^{2-} at the counter electrode, J. Phys. Chem. Let. 2 (2011) 2453–2460.
[24] K. Meng, G. Chen, K.R. Thampi, Metal chalcogenides as counter electrode materials in quantum dot sensitized solar cells: a perspective, J. Mater. Chem. A 3 (2015) 23074–23089.
[25] B. Yuan, Q. Gao, X. Zhang, L. Duan, L. Chen, Z. Mao, W. Lü, Reduced graphene oxide (RGO)/Cu_2S composite as catalytic counter electrode for quantum dot-sensitized solar cells, Electrochim. Acta 277 (2018) 50–58.
[26] Z. Du, Z. Pan, F.F. Santiago, K. Zhao, D. Long, H. Zhang, Y. Zhao, X. Zhong, J.S. Yu, J. Bisquert, Carbon counter-electrode-based quantum-dot-sensitized solar cells with certified efficiency exceeding 11%, J. Phys. Chem. Lett. 7 (2016) 3103–3111.
[27] C.X. Guo, H.B. Yang, Z.M. Sheng, Z.S. Lu, Q.L. Song, C.M. Li, Layered graphene/quantum dots for photovoltaic devices, Chem. Int. Ed. 49 (2010) 3014–3017.
[28] W.K. Bae, K. Char, H. Hur, S. Lee, Single-step synthesis of quantum dots with chemical composition gradients, Chem. Mater. 20 (2) (2008) 531–539.
[29] W.K. Bae, J. Kwak, J. Lim, D. Lee, M.K. Nam, K. Char, C. Lee, S. Lee, Multicolored light-emitting diodes based on all-quantum-dot multilayer films using layer-by-layer assembly method, Nano Lett. 10 (7) (2010) 2368–2373.
[30] J. Lim, S. Jun, E. Jang, H. Baik, H. Kim, J. Cho, Preparation of highly luminescent nanocrystals and their application to light-emitting diodes, Adv. Mater. 19 (2007) 1927–1932.
[31] B. Zhang, R. Hu, Y. Wang, C. Yang, X. Liu, K.T. Yong, Revisiting the principles of preparing aqueous quantum dots for biological applications: the effects of surface ligands on the physicochemical properties of quantum dots, RSC Adv. 4 (2014) 13805–13816.
[32] F. Wang, H. Dong, J. Pan, J. Li, Q. Li, D. Xu, One-step electrochemical deposition of hierarchical CuS nanostructures on conductive substrates as robust, high-performance counter electrodes for quantum-dot-sensitized solar cells, J. Phys. Chem. C 118 (2014) 19589–19598.
[33] S. Sonmezoglu, C. Akyurek, H. Akis, Modification of juglon dye as a sensitiser in dye-sensitised solar cells, IET Optoelectron. 8 (2014) 270–276.
[34] M.S. Hosseini, A. Pirouz, Study of fluorescence quenching of mercaptosuccinic acid-capped CdS quantum dots in the presence of some heavy metal ions and its application to Hg(II) ion determination, Luminescence 29 (7) (2014) 798–804.
[35] R.K. Ratnesh, M.S. Mehata, Investigation of biocompatible, protein sensitive highly luminescent quantum dots/nanocrystals of CdSe, CdSe/ZnS and CdSe/CdS, Spectrochim. Acta A 179 (2017) 201–210.
[36] A. Arivarasan, S. Bharathi, V. Vijayaraj, G. Sasikala, R. Jayavel, Evaluation of reaction parameters dependent optical properties and its photovoltaics performances of CdTe QDs, J. Inorg. Organomet. Polym. Mater. 28 (3) (2018) 1263–1275.
[37] Q. Yu, L.A. Jauregui, W. Wu, R. Colby, J. Tian, Z. Su, H. Cao, Z. Liu, D. Pandey, D. Wei, T.F. Chung, P. Peng, N.P. Guisinger, E.A. Stach, J. Bao, S.S. Pei, Y.P. Chen, Control and characterization of individual grains and grain boundaries in graphene grown by chemical vapour deposition, Nat. Mater. 10 (2011) 443–449.
[38] X. Li, W. Cai, J. An, S. Kim, J. Nah, D. Yang, R. Piner, A. Velamakanni, I. Jung, E. Tutuc, S.K. Banerjee, L. Colombo, R.S. Ruoff, Large-area synthesis of high-quality and uniform graphene films on copper foils, Science 324 (2009) 5932.
[39] T.F. Chung, T. Shen, H. Cao, L.A. Jauregui, W. Wu, Q. Yu, D. Newell, Y.P. Chen, Synthetic graphene grown by chemical vapor deposition on copper foils, Int. J. Mod. Phys. B 27 (2013) 1341002.
[40] A. Guermoune, T. Chari, F. Popescu, S.S. Sabri, J. Guillemette, H.S. Skulason, T. Szkopek, M. Siaj, Chemical vapor deposition synthesis of graphene on copper with methanol, ethanol, and propanol precursors, Carbon 49 (2011) 4204–4210.
[41] X. Li, C.W. Magnuson, A. Venugopal, J. An, J.W. Suk, B. Han, M. Borysiak, W. Cai, A. Velamakanni, Y. Zhu, L. Fu, E.M. Vogel, E. Voelkl, L. Colombo, R.S. Ruoff, Graphene films with large domain size by a two-step chemical vapor deposition process, Nano Lett. 10 (2010) 4328–4334.
[42] A. Reina, X. Jia, J. Ho, D. Nezich, H. Son, V. Bulovic, M.S. Dresselhaus, J. Kong, Large area, few-layer graphene films on arbitrary substrates by chemical vapor deposition, Nano Lett. 9 (2009) 30–35.
[43] D. Li, J. Ma, L. Zhou, Y. Li, C.W. Zou, Synthesis and characterization of Cu_2S nanoparticles by diethylenetriamine-assisted hydrothermal method, Optik 126 (2015) 4971–4973.
[44] Y. Su, X. Lu, M. Xie, H. Geng, H. Wei, Z. Yang, Y. Zhang, A one-pot synthesis of reduced graphene oxide–Cu_2S quantum dot hybrids for optoelectronic devices, Nanoscale 5 (2013) 8889–8893.
[45] H. Tang, Y. He, B. Li, J. Jung, C. Zhang, X. Liu, Z. Lin, Continuous crafting of uniform colloidal nanocrystals using an inert-gas-driven microflow reactor, Nanoscale 7 (2015) 9731–9737.
[46] C.C. Chen, W. Bao, C.C. Chang, Z. Zhao, C.N. Lau, S.B. Cronin, Raman spectroscopy of substrate-induced compression and substrate doping in thermally cycled graphene, Phys. Rev. B 85 (2012) 035431.
[47] G. Chen, S. Bandow, E.R. Margine, C. Nisoli, A.N. Kolmogorov, V.H. Crespi, R. Gupta, G.U. Sumanasekera, S. Iijima, P.C. Eklund, Chemically doped double-walled carbon nanotubes: cylindrical molecular capacitors, Phys. Rev. Lett. 90 (2003) 257403.
[48] A. Pan, R. Yu, S. Xie, Z. Zhang, C. Jin, B. Zou, ZnO flowers made up of thin nanosheets and their optical properties, J. Cryst. Growth 282 (2005) 165–172.
[49] Y. Yin, A.P. Alivisatos, Colloidal nanocrystal synthesis and the organic–inorganic interface, Nature 437 (2005) 664–670.
[50] M. Peng, L.L. Ma, Y.G. Zhang, M. Tan, J.B. Wang, Y. Yu, Controllable synthesis of self-assembled Cu_2S nanostructures through a template-free polyol process for the degradation of organic pollutant under visible light, Mater. Res. Bull. 44 (2009) 1834–1841.
[51] S. Li, K. Yu, Y. Wang, Z. Zhang, C. Song, H. Yin, Q. Ren, Z. Zhu, Cu_2S@ZnO hetero-nanostructures: facile synthesis, morphology-evolution and enhanced photocatalysis and field emission properties, CrystEngComm. 15 (2013) 1753–1761.
[52] Y. Li, H.X. Zhang, F.T. Liu, X.F. Dong, X. Li, C.W. Wang, New design of oriented NiS nanoflower arrays as platinum-free counter electrode for high-efficient dye-sensitized solar cells, Superlattice Microst. 125 (2019) 66–71.
[53] H.J. Kim, T.B. Yeo, S.K. Kim, S.S. Rao, A.D. Savariraj, K. Prabakar, V. Chandu, V.M. Gopi, Optimal-temperature-based highly efficient NiS counter electrode for quantum-dot-sensitized solar cells, Eur. J. Inorg. Chem. 26 (2014) 4281–4286.
[54] S. Hou, X. Cai, H. Wu, X. Yu, M. Peng, K. Yan, D. Zou, Nitrogen-doped graphene for dye-sensitized solar cells and the role of nitrogen states in triiodide reduction, Energy Environ. Sci. 6 (2013) 3356–3362.
[55] V.V.M. Chandu Gopi, M. Venkata-Haritha, S.K. Kim, S.S. Rao, D. Punnoose, H.J. Kim, Highly efficient and stable quantum dot-sensitized solar cells based on a Mn-doped CuS counter electrode, RSC Adv. 5 (2015) 2963–2967.
[56] S. Jiao, J. Du, Z. Du, D. Long, W. Jiang, Z. Pan, Y. Li, X. Zhong, Nitrogen-doped mesoporous carbons as counter electrodes in quantum dot sensitized solar cells with a conversion efficiency exceeding 12%, J. Phys. Chem. Lett. 8 (2017) 559–564.
[57] E. Vijayakumar, V.H.V. Quy, J.M. Kwon, J. Chae, J.H. Kim, S.H. Kang, H. Kim, K.S. Ahn, Enhanced electrocatalytic activity of Cu_2S-polyaniline heterostructure counter electrode for quantum dot-sensitized solar cells, J. Electrochem. Soc. 164 (12) (2017) F1211–F1215.
[58] S. Zhou, Q. Jiang, J. Yang, W. Chu, W. Li, X. Li, Y. Hou, J. Hou, Regulation of microstructure and composition of cobalt selenide counter electrode by electrochemical atomic layer deposition for high performance dye-sensitized solar cells, Electrochim. Acta 220 (2016) 169–175.